ACS OMEGA

http://pubs.acs.org/journal/acsodf

Article

Synthesis of TiO_2/Nanozeolite Composites for Highly Efficient Photocatalytic Oxidation of Propene in the Gas Phase

Javier Fernández-Catalá, Miriam Sánchez-Rubio, Miriam Navlani-García, Ángel Berenguer-Murcia, and Diego Cazorla-Amorós*

Cite This: *ACS Omega* 2020, 5, 31323−31331

Read Online

ACCESS | Metrics & More | Article Recommendations

ABSTRACT: In this work, we reported the preparation of composites based on titania (TiO_2) and Zeolite Socony Mobil-5 (ZSM-5) nanozeolite, following two approaches (i.e., incorporating the presynthesized zeolite in the synthesis medium of TiO_2 and incorporating presynthesized TiO_2 in the synthesis medium of ZSM-5). The materials synthesized were characterized by X-ray fluorescence (XRF), X-ray diffraction (XRD), nitrogen adsorption, X-ray photoelectron spectroscopy (XPS), ultraviolet−visible spectroscopy (UV−vis), transmission electron microscopy (TEM), scanning electron microscopy (SEM), and energy-dispersive X-ray (EDX) spectrometry analysis, and their photocatalytic activities were assessed in the oxidation of propene in the gas phase. It was observed that the synthesis methodology affects the final properties of the composite, which ultimately affected their photocatalytic performance in the studied application. It was found that the Nano-ZSM5/TiO_2 composite was the most active among the investigated samples, which was attributed to the intimate contact between the two components of the composite, the preserved properties of the photocatalytic active phase in the final material, and the positive contribution of the nanozeolite by increasing the local concentration of propene.

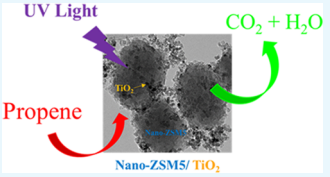

1. INTRODUCTION

Volatile organic compounds (VOCs) abatement is still one of the important challenges of our society since these contaminants are very harmful for the environment and human health.[1−5] These compounds can be present in indoor ambient and are responsible for a disease known as "sick house syndrome".[6,7] An interesting approach for VOC abatement is the use of photocatalytic reactions, which can totally remove these types of contaminants at low temperature, atmospheric pressure, and low concentration.[8−10] Propene can be used as a model molecule to study the low-molecular-weight VOC abatement using a photocatalytic methodology.[11−14] Titanium oxide (TiO_2) has been the most widely investigated photocatalyst in the last decades, which is due to its interesting properties such as low cost, chemical stability, and resistance to photocorrosion. For this reason, TiO_2 has been extensively used in different photocatalytic applications both in gas and liquid phases (i.e., pollutant removal, water splitting, and CO_2 reduction, among others[15,16]). Nevertheless, TiO_2 presents some limitations related to its low absorption in the visible light range, a electron−hole pair (e^-−h^+) recombination rate, and a low surface area, which limits its photocatalytic activity.[17,18]

Achieving TiO_2 with well-developed porosity has been a common approach considered to improve its photocatalytic activity.[19,20] Another interesting approach that has been tackled is the fabrication of TiO_2/adsorbent composites or supporting TiO_2 on adsorbents of diverse natures (i.e., carbon materials,[21,22] silica,[23−25] zeolites,[26,27] MOFs,[28−30] etc.). The resulting materials display enhanced performance, which results from their improved adsorption properties. Such properties allow the adsorption of molecules on the composite, which is followed by diffusion to the photocatalytic active sites where the photocatalytic reaction occurs.[31−33] Among the adsorbents investigated, the use of zeolites has received significant attention in the last years. This derives from their interesting properties such as the possibility to vary the chemical composition, high surface area, modulation of pores size, photochemical stability, thermal and chemical inertness, and transparency to ultraviolet−visible (UV−vis) radiation above 240 nm.[26,34]

In this sense, several studies addressing the use of TiO_2/zeolites for various photocatalytic applications can be found. For instance, Liu et al. were pioneers in the synthesis of TiO_2/zeolites hybrids. They studied the TiO_2/zeolites composite synthesis by TiO_2 incorporation inside zeolite Y cavities through ion exchange.[35] The same authors prepared TiO_2 encapsulated within zeolite Y, mordenite, or zeolite L, and the resulting materials were used for the photoreduction of methyl viologen to a methyl viologen radical cation. It was found that the encapsulated TiO_2 had a particle size in the nanometer

Received: September 30, 2020
Accepted: November 13, 2020
Published: November 25, 2020

https://dx.doi.org/10.1021/acsomega.0c04793
ACS Omega 2020, 5, 31323−31331

scale, which was responsible for the modified properties of TiO_2.[36] Sampath et al. observed complete mineralization of pyridine with a zeolite-supported photocatalyst consisting of 75 wt % TiO_2 and 25 wt % mordenite, which had better catalytic activity than pure TiO_2. They also observed diffusional problems of pyridine within the zeolite-supported photocatalyst when the thickness of the photocatalyst exceeded the penetration illumination depth.[37] Takeuchi et al. reported an interesting effect of the hydrophobicity of zeolites in TiO_2/Zeolite Socony Mobil-5 (ZSM-5) systems. It was observed that the composites with low content of Al_2O_3 in the zeolite (high hydrophobic zeolite) showed good photocatalytic activity, indicating that zeolites with hydrophobic properties promoted the photocatalytic activity of the TiO_2/HZSM-5 systems toward acetaldehyde degradation.[38] The same group observed that toluene or benzene molecules strongly interacted with the Na^+ or H^+ sites of the ultrastable Y (USY) zeolites and thus could not diffuse toward the TiO_2 surfaces. However, these molecules interacted weakly with the surface silanol groups of the USY zeolite and can easily diffuse toward the TiO_2 surfaces, resulting in high photocatalytic reactivity for the oxidation of toluene and benzene.[39] Kamegawa et al. observed that the use of fluorine-containing TiO_2 precursor for the synthesis of hybrids (TiO_2/Y zeolite) improved the photocatalytic performance of composites in the degradation of 2-propanol in water due to the different adsorption properties of the hybrids and the crystallinity properties of modified TiO_2.[40] Jansson et al. showed that an adequate balance between the surface area and the adsorption ability of TiO_2−zeolite composites is needed to obtain a high photocatalytic activity toward the degradation of formaldehyde and trichloroethylene in the gas phase.[27] The same group reported on the synergetic effect between TiO_2 and ZSM-5 zeolite when both phases had been in intimate contact and its importance in the removal of formaldehyde or trichloroethylene in the gas phase.[41] Huang et al. reported that a TiO_2/ZSM-5 catalyst prepared by the sol−gel method showed better photocatalytic activity for VOC degradation (benzene) under UV irradiation compared to commercial TiO_2 (P25).[42]

Another important factor that can affect the photocatalytic activity of the TiO_2/nanozeolite composites is the crystal size of both components (TiO_2 and zeolites) present in the composites. In this sense, the effect of the TiO_2 crystal size in pure TiO_2 or in the TiO_2/nanozeolite composites has been studied in photocatalysis.[19,20,36,40] However, the effect of zeolite crystal size in the final photocatalytic performance of such composites has been less profusely investigated, even though this parameter has a great effect in the catalytic activity of the bare zeolite in thermal catalysis, which is due to the fact that zeolites with smaller crystal size have a larger exposed surface area.[43,44]

With this in mind, the objective of the present study is the evaluation of the photocatalytic activity of composite materials constituted by TiO_2 and ZSM-5 nanozeolite (crystal size of ∼120 nm) for the abatement of VOCs at low concentration, using propene as a model molecule for low-molecular-weight VOCs. Previous studies reported that ZSM-5 zeolite (MFI-type framework) is an outstanding adsorbent material for propene molecules, which has been attributed to its characteristic adsorption sites (i.e., sinusoidal channel, straight channel, and channel intersection).[45−47] Such adsorption properties, combined with the photocatalytic activity of TiO_2, make TiO_2-ZSM-5 composites interesting candidates for the application addressed herein.[38,42] To investigate the effect of the synthesis conditions in the final photocatalytic performance, various composites were prepared focusing on the possible loss of the catalytic activity of TiO_2 due to its blocking or degradation, which is an issue that has not been widely described in the literature. Moreover, the effect of the zeolite crystal size in the composite was also explored by comparing the performance of both commercial ZSM-5 zeolite (crystal size of ∼290 nm) and the as-prepared ZSM-5 nanozeolite since this effect has been less extensively investigated in photocatalytic application with these kinds of composites.

2. RESULTS AND DISCUSSION

2.1. Characterization of the Composites. This section includes the results and discussion concerning the characterization of the prepared Nano-ZSM5/TiO_2, TiO_2/Nano-ZSM5, and Com-ZSM5/TiO_2 composites and the pure TiO_2, Nano-ZSM5, and Com-ZSM5 for comparison purposes (see Section 4.2).

X-ray fluorescence (XRF) analysis shows the presence of TiO_2 and zeolite in all composites prepared in this study. The Nano-ZSM5/TiO_2 composite (presynthesized nanozeolite[48] incorporated in the TiO_2 synthesis medium) is composed of 56 wt % TiO_2 and 44 wt % Nano-ZSM5, while the TiO_2/Nano-ZSM5 composite (presynthesized TiO_2[49] incorporated in nanozeolite synthesis medium) has a much lower proportion of TiO_2 (19 wt % of TiO_2 and 81 wt % of Nano-ZSM5), which indicates that the TiO_2 incorporated in the medium used for the synthesis of the zeolite may be dissolved or degraded by some of the reagents, such as NaOH under the synthesis conditions.[50] The Com-ZSM5/TiO_2 composite (commercial zeolite incorporated in the TiO_2 synthesis medium) is composed of 60 wt % of TiO_2 and 40 wt % of Com-ZSM5. The amount of TiO_2 and zeolite obtained in the Com-ZSM5/TiO_2 composite is similar to that obtained for the Nano-ZSM5/TiO_2 sample because in both composites, the same synthesis methodology was followed (See Section 4.2).

The X-ray diffraction (XRD) patterns of the composites and the pure phases, TiO_2 with hierarchical porosity and ZSM-5 zeolite, are depicted in Figure 1. As it has been previously reported, TiO_2 with hierarchical porosity only shows the characteristic peaks ascribed to the anatase phase.[49] All of the composites displayed the peaks attributed to the presence of TiO_2 and nanozeolite. The obtained diffractograms indicate that the TiO_2/Nano-ZSM5 composite has a larger proportion of nanozeolite, while a larger proportion of TiO_2 is present in

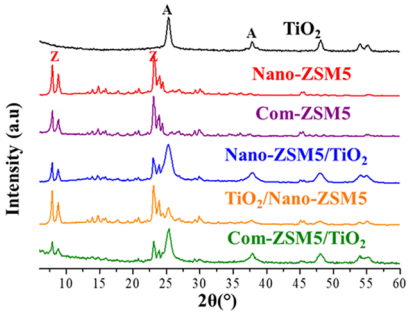

Figure 1. XRD patterns of TiO_2/nanozeolite composites. The diffractograms of TiO_2, ZSM-5 nanozeolite, and commercial ZSM-5 zeolite are shown for comparison. Key: A = anatase phase (TiO_2) and Z = ZSM-5 nanozeolite.

https://dx.doi.org/10.1021/acsomega.0c04793
ACS Omega 2020, 5, 31323−31331

the Nano-ZSM5/TiO_2 composite, which is in good agreement with XRF results. The Com-ZSM5/TiO_2 composite shows the same crystallite phases (anatase and ZSM-5 phases) as those observed in the Nano-ZSM5/TiO_2 composite (Figure 1).

The results of the N_2 adsorption−desorption measurements at −196 °C are depicted in Figure 2 and the textural properties

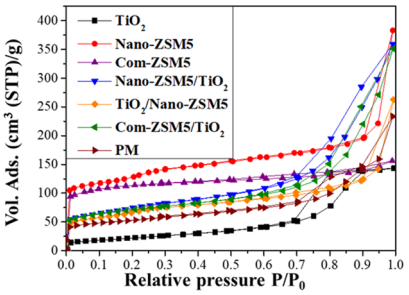

Figure 2. N_2 isotherms at −196 °C of TiO_2/nanozeolite composites. N_2 isotherms at −196 °C of TiO_2, ZSM-5 nanozeolite, ZSM-5 commercial zeolite, and the physical mixture of both components (TiO_2 and Nano-ZSM5) are shown for comparison purposes.

Table 1. Textural Properties of the Composites[a]

support	surface area (m^2/g)	V_{DR} (cm^3/g)	$V_{mesopores}$ (cm^3/g)	V_t (cm^3/g)
TiO_2	83	0.03	0.19	0.22
Nano-ZSM5	431	0.19	0.16	0.35
Com-ZSM5	425	0.17	0.04	0.21
Nano-ZSM5/TiO_2	254	0.10	0.36	0.46
TiO_2/Nano-ZSM5	234	0.10	0.12	0.22
Com-ZSM5/TiO_2	248	0.10	0.30	0.40
PM	263	0.08	0.17	0.25

[a]Data for TiO_2, Nano-ZSM5, Com-ZSM5, and PM are shown for comparison purposes.

as collected in Table 1. The N_2 physisorption isotherm of TiO_2 showed a combination of type I and IV isotherms, which is typical of mesoporous materials with a certain degree of microporosity, as previously reported by our research group.[49] Both commercial ZSM-5 zeolite and ZSM-5 nanozeolite show a type I isotherm[48] but the last one shows a slightly larger contribution of micropores than the commercial counterpart. ZSM-5 nanozeolite displays some slope from relative pressures higher than 0.2 and a small hysteresis loop at high relative pressures, which is due to the presence of a small number of mesopores and to the adsorption of N_2 in the interparticle space. TiO_2/Nano-ZSM5 and Nano-ZSM5/TiO_2 composites show a combination of isotherms from TiO_2 and ZSM-5. TiO_2/Nano-ZSM5 shows a less marked hysteresis than Nano-ZSM5/TiO_2 due to the lower content of TiO_2 in the TiO_2/Nano-ZSM5 composite. Concerning the Com-ZSM5/TiO_2 composite, this composite presents a combination of isotherms between TiO_2 and ZSM-5 obtaining type I and IV isotherms, as it was observed in the Nano-ZSM5/TiO_2 composite.

Composite materials containing ZSM-5 nanozeolite have adequately developed porosity, confirming the suitability of the experimental procedure carried out in the synthesis of the studied materials (Table 1). As previously mentioned, the TiO_2/Nano-ZSM5 and PM samples present a lower volume of mesopores compared to the Nano-ZSM5/TiO_2 sample (Table 1), which can be attributed to the lower content of TiO_2 in the first and to the milling process used in the synthesis of the second material (PM). Concerning the Com-ZSM5/TiO_2 composite, it shows a slightly lower volume of mesopores than Nano-ZSM5/TiO_2.

Ti 2p and O 1s X-ray photoelectron spectroscopy (XPS) spectra for the composites are shown in Figure 3. Figure 3A depicts the Ti 2p spectra of TiO_2 and for Nano-ZSM5/TiO_2 and TiO_2/Nano-ZSM5 composites. Concerning bare TiO_2, Ti present in the sample TiO_2 with hierarchical porosity is as Ti(IV) (Ti $2p_{1/2}$ (464−465 eV) and Ti $2p_{3/2}$ (458.5−459 eV) transitions are in agreement with Ti(IV)[51]). The Ti 2p XPS spectrum of the Nano-ZSM5/TiO_2 composite (Figure 3A) shows peaks corresponding to Ti $2p_{1/2}$ (464−465 eV) and Ti $2p_{3/2}$ (458.5−459 eV) transitions, indicating that Ti is in a Ti(IV) form.[52,53] However, Ti is almost not detected in sample TiO_2/Nano-ZSM5, which is not only due to the low TiO_2 content in this sample (19 wt % compared to 60 wt % in the other composite) but also due to the possibility that the TiO_2 phase can be encapsulated by Nano-ZSM5, considering the experimental method used (i.e., ZSM-5 precipitation on TiO_2 particles added to the reaction medium). In the Ti 2p XPS spectrum, a blue shift was observed in Nano-ZSM5/TiO_2 with respect to the peak of TiO_2. This might be due to sample charging under X-ray radiation, as it has been described in the literature.[53]

For a better understanding of the interaction between TiO_2 and ZSM-5 nanozeolite in the composites, O 1s XPS spectra are analyzed (Figure 3B). The Nano-ZSM5/TiO_2 composite shows the characteristic peaks of a Ti−O bond (529.6 eV) and a Si−O bond (533.4 eV), indicating the presence of TiO_2 and

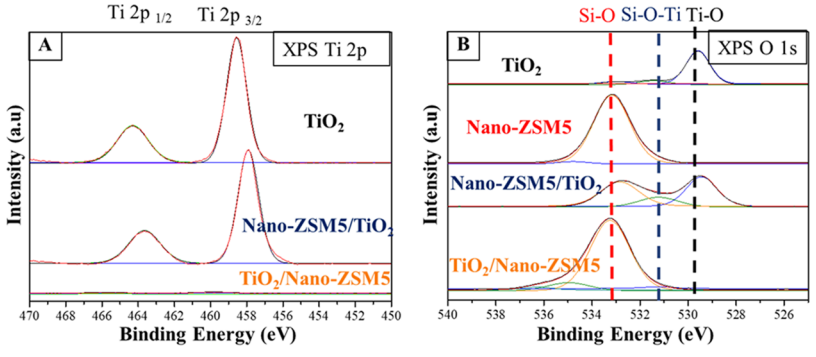

Figure 3. (A) Ti 2p XPS spectra of the composites and TiO_2 and (B) O 1s XPS spectra of the composites, TiO_2, and Nano-ZSM5.

https://dx.doi.org/10.1021/acsomega.0c04793
ACS Omega 2020, 5, 31323−31331

zeolite in the composite material, respectively.[54,55] Moreover, the Nano-ZSM5/TiO_2 composite shows a peak at 531.7 eV, which could be related to the presence of a Si−O−Ti bond due to good interaction between TiO_2 and the zeolitic phase. The TiO_2/Nano-ZSM5 composite only shows a characteristic peak at 533.4 eV (Si−O bond), which is ascribed to the zeolitic material, while signals related to TiO_2 are not detected. TiO_2 shows the characteristic peak of the Ti−O bond (529.6 eV) and a small peak at 531.4 eV, which is the characteristic of the organic matter present in the sample, although these materials have been calcined, and this value (531.4 eV) being very similar to the characteristic peak of the Si−O−Ti bond (531.7 eV).[55] From XRF and XRD, it can be concluded that TiO_2 is partially dissolved during the synthesis process and that the remaining TiO_2 present in the composite is covered by ZSM-5.

Figure 4 shows the UV−vis absorption spectra of the composites synthesized in this study and bare TiO_2. TiO_2/

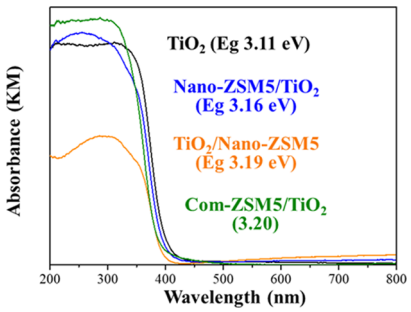

Figure 4. UV−vis absorption spectra and the band gap value (Eg) of the composites and bare TiO_2.

zeolite composites (TiO_2/Nano-ZSM5, Nano-ZSM5/TiO_2, and Com-ZSM5/TiO_2) have a similar absorption edge and band gap compared to the bare TiO_2 with hierarchical porosity, previously described by our research group.[49] This fact indicates the presence of the anatase phase in the materials (3.12 eV).[13] However, the composite TiO_2/Nano-ZSM5 shows lower absorption than the Nano-ZSM5/TiO_2 sample in the 200−350 nm range (UV light), possibly due to the encapsulation and/or partial dissolution of the TiO_2 phase.

Figure 5 includes the transmission electron microscopy (TEM) micrographs of the composites and pure components (i.e., TiO_2, ZSM-5 nanozeolite, and commercial ZSM-5 zeolite). Concerning the morphology of the zeolitic phase, TEM images show that the ZSM-5 nanozeolite (Figure 5B) has smaller crystallite size than commercial zeolite (Figure 5C). The histogram of the nanozeolite (counting 100 crystallites of ZSM-5) shows that it has a narrow crystallite size distribution and average crystallite size of 120 ± 16 nm. However, the commercial zeolite (counting 50 crystallites of ZSM-5) has a much wider crystallite size distribution and an average crystallite size of 290 ± 120 nm, with small crystallites of 60 nm up to larger ones of 500 nm in size.

As for the composites, all of them show the presence of both components but important differences were observed. The Nano-ZSM5/TiO_2 composite (Figure 5D) shows that there is a good dispersion of the TiO_2 phase on the ZSM-5 crystals, indicating good interaction between TiO_2 and nanozeolite in the Nano-ZSM5/TiO_2 composite, while the composite prepared by physically mixing the two solids shows a poorer dispersion of TiO_2 on the surface of the zeolite (Figure 5G).

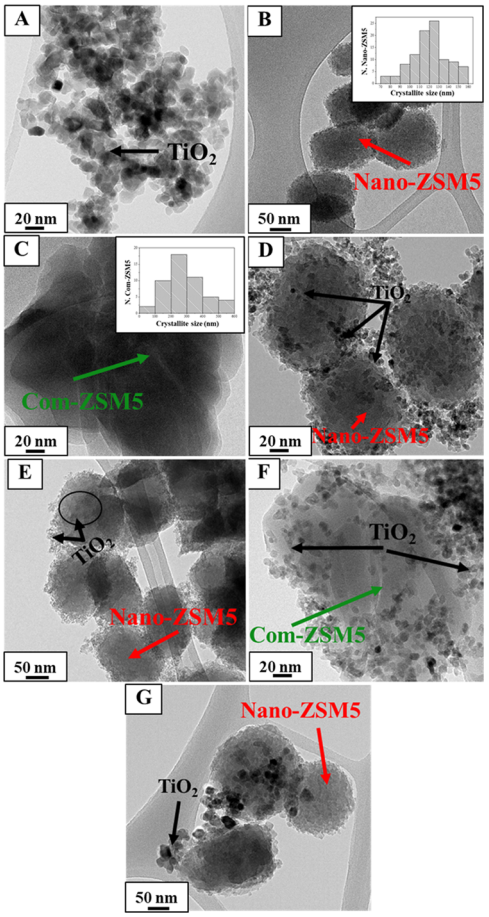

Figure 5. TEM images of the samples studied in this work: (A) TiO_2, (B) Nano-ZSM5 and its corresponding histograms by counting 100 particles of ZSM-5, (C) Com-ZSM5 and its corresponding histograms by counting 50 particles of ZSM-5, (D) Nano-ZSM5/TiO_2, (E) TiO_2/Nano-ZSM5, (F) Com-ZSM5/TiO_2, and the (G) physical mixture.

Such good dispersion of TiO_2 on the nanozeolite crystals can be related to the higher volume of mesopores (Table 1), which increases the number of nucleation sites for Ti species during the growth of TiO_2, thus leading to an improved interaction between TiO_2 and nanozeolite components with respect to the Com-ZSM5/TiO_2 composite (Figure 5F). Moreover, this interaction can be due to the employed sol−gel methodology, which can favor the interaction between the components since TiO_2 can grow on the Si−OH anchoring points of the zeolite, leading to a better interaction in the composite than in the sample prepared by a physical mixture. The micrographs of the TiO_2/Nano-ZSM5 composite (Figure 5E) show a morphology, which is very similar to that of the pure zeolite (Figure 5B), suggesting that ZSM-5 nanozeolite is covering the TiO_2 phase.

Scanning electron microscopy (SEM) images and energy-dispersive X-ray (EDX) spectrometry mapping images of the Nano-ZSM5/TiO_2, TiO_2/Nano-ZSM5, and PM composites are depicted in Figures 6 and 7, respectively. The Nano-ZSM5/TiO_2 composite (presynthesized nanozeolite incorporated in the TiO_2 synthesis medium) shows that the TiO_2 phase almost completely covers the nanozeolite (Figures 6A and 7A), which is in agreement with the previously discussed XPS results. In the case of the TiO_2/Nano-ZSM5 composite

https://dx.doi.org/10.1021/acsomega.0c04793
ACS Omega 2020, 5, 31323−31331

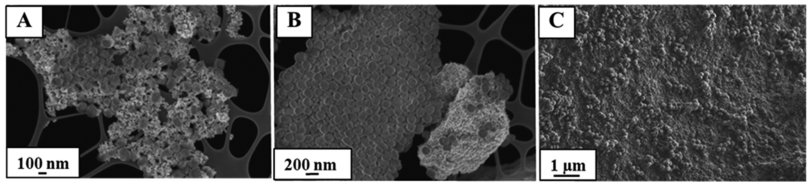

Figure 6. FE-SEM images: (A) Nano-ZSM5/TiO_2, (B) TiO_2/Nano-ZSM5, and (C) PM.

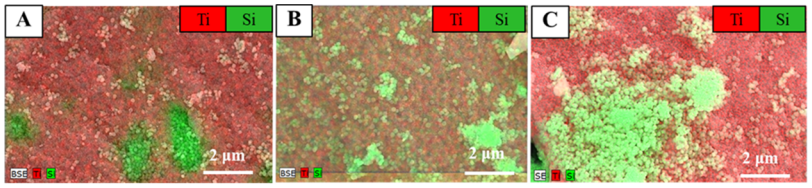

Figure 7. EDX images mapping: (A) Nano-ZSM5/TiO_2, (B) TiO_2/Nano-ZSM5, (C) PM.

(presynthesized TiO_2 incorporated in nanozeolite synthesis medium), ZSM-5 nanozeolite partially covers the surface of the TiO_2 phase (Figures 6B and 7B). However, the composite prepared from a physical mixture of both components (PM) displayed a heterogeneous distribution of both phases (Figures 6C and 7C).

Breakthrough curve measurements of propene (Table 2) show that zeolites have an adsorption capacity, which is two orders of magnitude higher than that of TiO_2. In addition, the propene adsorption capacity of the nanozeolite is slightly higher than that of the commercial counterpart.

Table 2. Propene Adsorption Capacity (mmoles of Propene/g Adsorbent) of TiO_2, Nano-ZSM5, and Com-ZSM5

material	mmoles C_3H_6 ads/g adsorbent
TiO_2	0.0004
Nano-ZSM5	0.0153
Com-ZSM5	0.0107

2.2. Photocatalytic Activity. In this section, the results of propene conversion and the CO_2 production rate of the materials studied in the present work are included, focusing on the effect of the synthesis methodology used for composite preparation and the synergetic effect between TiO_2 and ZSM-5 zeolite. Besides, the effect of the zeolite crystal size (290 ± 120 and 120 ± 16 nm, for commercial ZSM-5 and ZSM-5 nanozeolite, respectively) in the photocatalytic activity displayed by the composites is also included in this section.

The photocatalytic results of the composites and bare TiO_2 are shown in Figure 8. The Nano-ZSM5/TiO_2 photocatalyst shows the best propene conversion among the investigated samples, even being superior to pure TiO_2 (active phase), which indicates that the incorporation of the nanozeolite has a positive effect on the final activity. However, TiO_2/Nano-ZSM5 material presents a low propene conversion because this composite has a low amount of TiO_2 (see XRF analysis described in Section 2.1). Moreover, TiO_2 (active phase) might have been deteriorated in the zeolite synthesis medium or blocked by the growing nanozeolite, causing the low propene conversion displayed by this composite. The superior performance of the Nano-ZSM5/TiO_2 composite is further evidenced by normalizing the CO_2 production rate per mol of the TiO_2 active phase. This observation confirms the importance of the synthesis methodology used for the composite preparation. In this sense, the TiO_2/Nano-ZSM5 composite displays a low CO_2 production rate since TiO_2, which is the photocatalytic active phase, is deteriorated during the composite preparation[51] or unaccessible due to the zeolite phase covering TiO_2.

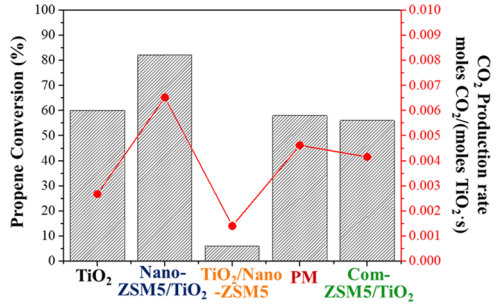

Figure 8. Comparison of propene conversion and CO_2 production rates for the composites studied in this work. The propene conversion and CO_2 production rates of TiO_2 and the physical mixture (PM) are also shown for comparison purposes.

With the aim of studying the synergetic effect between TiO_2 and zeolite in the composites, a physical mixture of both materials (PM) was tested. The PM composite shows a similar propene conversion to TiO_2 despite the PM having 56 wt % of TiO_2 (active phase), indicating that the presence of zeolite in the composite improves the final performance, even in this sample in which there is no intimate contact between both phases. Comparing PM with the Nano-ZSM5/TiO_2 composite in terms of propene conversion, the Nano-ZSM5/TiO_2 composite shows higher conversion, indicating a synergetic effect between TiO_2 and ZSM-5 nanozeolite due to good interaction between both components in the composite with respect to the composite prepared by a physical mixture since the employed sol−gel methodology may favor the interaction between the components since TiO_2 can grow on the Si−OH anchoring points of the zeolite, leading to a better interaction in the composite than in the sample prepared by a physical mixture.[2,56] When analyzing the CO_2 production rate per mol of TiO_2, Nano-ZSM5/TiO_2 and PM composites show higher values than those achieved with pure TiO_2, corroborating the positive effect of the incorporation of the nanozeolite in the composite. Such enhancement observed upon using TiO_2/Nanozeolite composites might be related to the zeolite

https://dx.doi.org/10.1021/acsomega.0c04793
ACS Omega 2020, 5, 31323−31331

adsorption properties, see Table 2, which leads to the increase in the concentration of propene molecules near the photocatalytic active sites, thus improving the final performance of the materials.

It should be noted that the catalytic tests of propene oxidation for the composites and pure materials were performed until steady-state conditions were reached. This means that the zeolite pores act as reservoirs for propene, which is continuously adsorbed and oxidized. Thus, the effect of the adsorption is to increase the propene concentration in the vicinity of the reaction sites, as it has been previously indicated. If there was only adsorption, the removal of propene would only be observed until the saturation of the adsorbent is reached. Since adsorption is coupled with photocatalytic oxidation, the complete removal of propene is reached during the complete time of the reaction studied. Then, the contribution of a pure adsorption process to the continuous complete oxidation of propene during the time of the experiments at a steady state is negligible.

Regarding the effect of using a nanozeolite in the final photocatalytic performance, it was observed that the results achieved by the Com-ZSM5/TiO_2 composite with commercial ZSM-5 show a moderate improvement as compared to the performance displayed by the pure TiO_2 phase, while a much significant enhancement was achieved by the Nano-ZSM5/TiO_2 composite. Such beneficial effect of using ZSM-5 nanozeolite can be attributed to the smaller and more homogeneous crystallite size of the Nano-ZSM5 shown in the composite, which favors a more exposed surface area and better contact between the TiO_2 and nanozeolite.[33,43]

Considering the results obtained in this study in terms of characterization of the samples and their performance in the photocatalytic oxidation of propene at low concentrations, the most promising outlook seems to be the following: (1) this work presents different strategies for the preparation of TiO_2 and zeolite (ZSM-5) composites, indicating that the synthesis methodology has a great effect on the final properties of the composite; (2) the TiO_2 phase of the composite is the catalytic active phase of the composite, and for this reason, it is important that TiO_2 is not degraded or blocked in any way during synthesis; (3) the synergetic effect between TiO_2 and zeolite takes place due to an intimate contact between both components. The zeolitic phase acts as the adsorbent for the propene molecules and this favors the final photoactivity of the resulting composites; and (4) the selection of a zeolite with interesting properties, such as small and homogenous crystallite size and a suitable porous structure, allows an improved photocatalytic activity of the composite.

For all of these reasons, the Nano-ZSM5/TiO_2 composite, prepared using an adequate synthesis methodology that does not affect the photocatalytic active phase, displays a remarkably higher photocatalytic activity than bare TiO_2. In this sense, the composite prepared using a nanozeolite with adequate porosity and homogenous and small crystallite size (Nano-ZSM5/TiO_2) showed the highest photocatalytic activity in the propene photooxidation in the gas phase at low concentration among investigated ones.

3. CONCLUSIONS

In this study, we studied the TiO_2/nanozeolite composites focusing on two different synthesis methodologies, either incorporating the presynthesized zeolite in the synthesis medium of TiO_2 or incorporating presynthesized TiO_2 in the synthesis medium of ZSM-5. We also studied the effect of using nanozeolite or commercial zeolite in the synthesis of the composites for photocatalytic applications. The obtained results give evidence that the synthesis methodology is an important factor in the preparation of TiO_2/Nanozeolite composites. It was observed that the composites prepared by incorporating the zeolite in the TiO_2 medium synthesis displayed better results toward the photodegradation of propene than those composites in which presynthesized TiO_2 was incorporated in the synthesis medium of ZSM-5 or the physical mixture of both components. The beneficial role of the zeolitic phase was related to its adsorption properties, which led to an increase in the concentration of propene molecules near the photocatalytic active sites, thus resulting in an enhanced performance compared with that of bare TiO_2.

It was also observed that the zeolite crystal size has an effect on the final performance of the composites in the studied application. Nano-ZSM5/TiO_2 showed a much superior performance than Com-ZSM5/TiO_2, which was ascribed to the smaller crystal size that is responsible for the larger exposed external surface area and better contact with the photoactive TiO_2 phase.

4. MATERIALS AND METHODS

4.1. Materials. Tetraethyl orthosilicate (TEOS, 98%, Sigma-Aldrich), aluminum isopropoxide (98%, Sigma-Aldrich), tetrapropylammonium hydroxide (TPAOH, 1 M, Sigma-Aldrich), sodium hydroxide (≥ 98%, Sigma-Aldrich), titanium-(IV) tetrabutoxide (TTB, 97%, Sigma-Aldrich), urea (99%, Merck), Pluronic F-127 (F-127, Sigma-Aldrich), glacial acetic acid (HAc, 99%, Sigma-Aldrich), formamide (FA, 99.5%, Sigma-Aldrich), absolute ethanol (EtOH, 99.8%, Fisher Scientific), commercial zeolite (NH_4-ZSM-5, Zeolyst International), and deionized water were used in the present work. All reactants were used as received, without further purification.

4.2. Sample Preparation. In this work, we have performed the preparation of TiO_2/Nanozeolite composites using two different synthesis approaches: In the first approach, a presynthesized ZSM-5 nanozeolite, which was prepared by following the protocol described by Nejad-Darzi,[48] was incorporated in the synthesis medium of TiO_2 with hierarchical porosity, previously described by our research group.[49] The resulting composite was denoted as Nano-ZSM5/TiO_2. In the second approach, the presynthesized TiO_2 with hierarchical porosity was incorporated in the synthesis medium of ZSM-5 nanozeolite.[48] The resulting composite was denoted as TiO_2/Nano-ZSM5. To obtain an insight into the effect of the zeolite crystal size, the first approach was also performed using commercial ZSM-5 zeolite in an acidic form. The resulting material was named as Com-ZSM5/TiO_2. The synthetic protocols are described below.

The first approach (preparation of Nano-ZSM5/TiO_2) was performed as follows. First, two solutions were prepared for the synthesis of TiO_2 with hierarchical porosity:[49] 5 g of the titanium precursor (titanium tetrabutoxide, TTB) was weighed and dissolved in 7.9 g of EtOH, and the mixture was stirred vigorously for 10 min ("solution A"). Then, in this order, 1.6 g of deionized water, 7.9 g of EtOH, 0.3 g of F-127, 0.4 g of FA, 0.4 g of urea, and 1.6 g of HAc were weighed and added in a separate vessel. The mixture was stirred for 10 min ("solution B"). Then, the previously synthesized and calcined (at 500 °C for 6 h) nanozeolite was incorporated in solution B and the resulting mixture was dispersed with an ultrasound probe

https://dx.doi.org/10.1021/acsomega.0c04793
ACS Omega 2020, 5, 31323−31331

(Bandelin SONOPULS HD 2200) for 5 min with a power of 660 W operating at 30% output power. Solution B with the dispersed nanozeolite was rapidly added dropwise into solution A under vigorous stirring. The resulting solution was transferred to a 40 mL autoclave and heated at 60 °C for 24 h and the temperature was later increased to 120 °C with a dwelling time of 24 h. The sample obtained was calcined at 500 °C for 6 h with a heating rate of 1 °C/min. The same synthesis steps were carried out for the preparation of Com-ZSM5/TiO_2 but using commercial ZSM-5 zeolite in an acidic form instead of ZSM-5 nanozeolite. Prior to the synthesis of the composite, the commercial zeolite (NH_4-ZSM-5) was calcined at 500 °C for 6 h to obtain the acidic form (HZSM-5).

The second approach (preparation of TiO_2/Nano-ZSM5) was performed as follows. ZSM-5 nanozeolite was synthesized by following the procedure described by Nedaj-Darzi et al.:[48] 0.24 g of aluminum isopropoxide was dissolved in 17.7 mL of TPAOH (1 M) solution with stirring, followed by addition of NaOH (0.0071 g) and distilled water (22.8 mL). TiO_2 (previously synthesized) was incorporated into that solution and the resulting mixture was dispersed with an ultrasound probe (Bandelin SONOPULS HD 2200) for 5 min with a power of 660 W operating at 30% output power. Afterward, 15.87 mL of tetraethyl orthosilicate (TEOS) was incorporated in the dispersion of TiO_2 and the mixture was stirred at ambient temperature for 24 h. After that, the gel obtained was stirred under reflux at 100 °C for 48 h. The resulting nanocrystals were centrifuged at 5000 rpm for 1 h, washed three times with distilled water, and dried at 90 °C overnight. The synthesized composite was calcined at 500 °C for 5 h.

We also prepared a physical mixture of both components (nanozeolite and TiO_2), mixing both components with an agate mortar, with the aim of studying the synergetic effect existing in the prepared TiO_2/nanozeolite composites. The resulting material was named as PM.

The individual components (i.e., TiO_2 with hierarchical porosity, ZSM-5 nanozeolite, and commercial ZSM-5 zeolite) were used as reference samples. The synthesis of TiO_2 with hierarchical porosity has been performed following the first approach[49] without the incorporation of the correspondent zeolite. The ZSM-5 nanozeolite was synthesized using the second approach[48] without the incorporation of the TiO_2. The commercial zeolite (NH_4-ZSM-5, Zeolyst International) was converted into its acidic form by calcining the ammonium zeolite at 500 °C for 6 h.

4.3. Sample Characterization. The composition of the composites was determined by X-ray fluorescence spectroscopy (XRF) using a PHILIPS MAGIX PRO spectrometer. The crystal phase composition and crystallinity of TiO_2 were determined by X-ray diffraction (XRD) analysis using a Miniflex II Rigaku with Cu Kα radiation and a scanning rate of 2°/min, in the 2θ range of 5−80°. Nitrogen adsorption−desorption isotherms were performed at −196 °C in an Autosorb-6B apparatus from Quantachrome Corporation. Prior to the analysis, samples were degassed at 250 °C for 4 h under vacuum. The Brunauer−Emmett−Teller (BET) surface area (S_{BET}) and total micropore volume (V_{DR}) were determined by applying the Brunauer−Emmett−Teller (BET) equation and the Dubinin−Raduskevich (DR) equation to the N_2 adsorption data obtained at −196 °C, respectively. Total pore volumes (V_t) were determined from the adsorbed nitrogen volume at a relative pressure of 0.95. The interaction between the TiO_2 and zeolite in the composites was analyzed by X-ray photoelectron spectroscopy (XPS) using a K-α spectrometer from Thermo-Scientific, equipped with an Al anode. The optical absorption properties were studied using a UV−vis/DR spectrometer (Jasco V-670). $BaSO_4$ was used as the reference standard and the reflectance signal was calibrated with a Spectralon standard (Labsphere SRS-99-010, 99% reflectance). The absorption edge wavelength was estimated from the intercept at zero absorbance of the high slope portion of each individual spectrum in the range 200−800 nm (absorbance method). Then, the band gap was calculated[57] with the following equation (eq 1)

$$E_g = \frac{1239.8}{\lambda} \quad (1)$$

where E_g is the band gap energy (eV) and λ is the edge wavelength (nm).

The morphology of the samples was checked by transmission electron microscopy (TEM) and field-emission scanning electron microscopy (FE-SEM). TEM images were taken using a JEOL JEM-2010 equipment. FE-SEM images were taken using a ZEISS, Merlin VP Compact, which has a built-in microanalysis system using an energy-dispersive X-ray spectrometer (EDX) (Bruker Quantax 400) to perform elemental mapping of Si and Ti species present in the samples.

Breakthrough curve measurements of propene were performed at a laboratory scale in a fixed-bed reactor system (20 mm of diameter) coupled to a mass spectrometer (Balzers, OmniStar), using the catalytic test conditions without light irradiation. This was carried out to know the propene adsorption capacity of the samples under the same conditions as the catalytic test. The weight of the adsorbent was 0.11 g and a flow of 30 (STP) mL/min of the propene (100 ppmv in air) using a calibrated gas cylinder was supplied by Carburos Metálicos, S.A. The adsorption temperature was 25 °C.

4.4. Catalytic Tests. The photocatalytic performance in propene photooxidation at low concentration of the different photocatalysts studied in this work was assessed using an experimental setup, previously reported by our research group.[58] This experimental setup is based on a vertical quartz reactor where the photocatalyst was placed on a quartz wool bed. The reactor has the following dimensions: 50 mm in height, 20 mm in diameter, and a quartz wool support of approximately 10 mm in height. A commercial UV lamp with the radiation peak at 365 nm (Philips, TL 8W/05 FAM, 1 W) was used to irradiate the photocatalyst in a parallel position at a distance of 1 cm. The UV lamp and quartz reactor with the photocatalyst were surrounded by a cylinder covered with an aluminum foil.

The photocatalytic tests were performed under flow conditions at room temperature and with a low concentration of propene (100 ppmv in air), using a calibrated gas cylinder supplied by Carburos Metálicos, S.A. First, the photocatalyst (0.11 g) was incorporated in the quartz reactor, and then the reactor was purged with a helium flow of 30 (STP) mL/min to clean the surface of the catalyst. The propene-containing stream of 30 (STP) mL/min was passed through the calibration setup until the propene concentration was stable (∼3 h) to calibrate the concentration of propene. After that, propene was passed through the reactor with the photocatalyst, and the lamp was switched on at the same time and kept working until steady-state conditions were reached (∼ 3 h).

https://dx.doi.org/10.1021/acsomega.0c04793
ACS Omega 2020, 5, 31323−31331

The outlet gas was continuously analyzed by a mass spectrometer (Balzers, Thermostar GSD 301 01).

Propene conversion was calculated using the following expression (eq 2)

$$\text{propene conversion}(\%) = \frac{C_{\text{initial}_{C_3H_6}} - C_{\text{steady state}_{C_3H_6}}}{C_{\text{initial}_{C_3H_6}}} \times 100 \quad (2)$$

where $C_{\text{initial } C_3H_6}$ is the initial propene concentration, (100 ppmv), and $C_{\text{steady state } C_3H_6}$ is the propene concentration at steady-state conditions in the outlet gas when the UV light is switched on. The CO_2 production rate per mol of the active phase (TiO_2) was calculated using the following expression (eq 3), with the aim to normalize the results with the amount of TiO_2

$$CO_2 \text{ production rate} = \frac{q_{\text{gen}}}{n} \quad (3)$$

where q_{gen} is the molar flow rate of CO_2 generated (moles CO_2/s) and n is the moles of the photocatalyst (moles of TiO_2). Total oxidation of propene to CO_2 takes place under reaction conditions[58] so that there is no effect of accumulation of byproducts on the catalytic sites.

AUTHOR INFORMATION

Corresponding Author

Diego Cazorla-Amorós − *Materials Institute and Inorganic Chemistry Department, University of Alicante, E-03080 Alicante, Spain;* orcid.org/0000-0001-5745-4271; Email: cazorla@ua.es

Authors

Javier Fernández-Catalá − *Materials Institute and Inorganic Chemistry Department, University of Alicante, E-03080 Alicante, Spain*

Miriam Sánchez-Rubio − *Materials Institute and Inorganic Chemistry Department, University of Alicante, E-03080 Alicante, Spain*

Miriam Navlani-García − *Materials Institute and Inorganic Chemistry Department, University of Alicante, E-03080 Alicante, Spain*

Ángel Berenguer-Murcia − *Materials Institute and Inorganic Chemistry Department, University of Alicante, E-03080 Alicante, Spain;* orcid.org/0000-0003-3204-801X

Complete contact information is available at: https://pubs.acs.org/10.1021/acsomega.0c04793

Author Contributions

J.F.-C., D.C.-A., and A.B.-M. conceived and designed the experiments; M.S.-R. and J.F.-C. performed the experiments; J.F.-C., M.S.-R., M.N.-G., A.B.-M., and D.C.-A analyzed the data; J.F.C. and M.N.G. wrote the original draft version; M.N.-G., A.B.-M., and D.C.-A revised and edited the original draft; and M.N.-G., A.B.-M., and D.C.-A. supervised the research.

Notes

The authors declare no competing financial interest.

ACKNOWLEDGMENTS

The authors thank Ministerio de Ciencia Innovación y Universidades and FEDER (Project RTI2018-095291-B-I00) and the Generalitat Valenciana (PROMETEOII/2018/076) for financial support. J.F.-C. thanks MINECO for a researcher formation grant (BES-2016-078079). M.N.-G. gratefully acknowledges Generalitat Valenciana and Plan GenT (CDEIGENT/2018/027) for the postdoctoral grant.

REFERENCES

(1) Rafson, H. J. *Odor and VOC Control Handbook*, 1st ed.; McGraw Hill: New York, NY, U.S.A., 1998.

(2) Olsen, E.; Nielsen, F. Predicting vapour pressures of organic compounds from their chemical structure for classification according to the VOC-directive and risk assessment in general. *Molecules* **2001**, *6*, 370−389.

(3) Manahan, S. E. *Environmental Chemistry*, 8th ed.; CRC Press: Boca Raton, FL, U.S.A., 2004.

(4) Abbas, N.; Hussain, M.; Russo, N.; Saracco, G. Studies on the activity and deactivation of novel optimized TiO_2 nanoparticles for the abatement of VOCs. *Chem. Eng. J.* **2011**, *175*, 330−340.

(5) Veerapandian, S.; Leys, C.; Geyter, N.; Morent, R. Abatement of VOCs using packed bed non-thermal plasma reactors: A review. *Catalyst* **2017**, *7*, No. 113.

(6) Rodhe, H. A comparison of the contribution of various gases. *Science* **1990**, *248*, 1217−1219.

(7) Kamal, M. S.; Razzak, S. A.; Hossain, M. M. Catalytic oxidation of volatile organic compounds (VOCs) - A review. *Atmos. Environ.* **2016**, *140*, 117−134.

(8) Kaneko, M.; Okura, I. *Photocatalysis: Science and Technology*, Springer: Berlin, Germany, 2020.

(9) Kong, J.; Li, G.; Wen, M.; Chen, J.; Liu, H.; An, T.; Catal, J. The synergic degradation mechanism and photothermocatalytic mineralization of typical VOCs over $PtCu/CeO_2$ ordered porous catalysts under simulated solar irradiation. *J. Catal.* **2019**, *370*, 88−96.

(10) Kong, J.; Xiang, Z.; Li, G.; An, T. Introduce oxygen vacancies into CeO_2 catalyst for enhanced coke resistance during photothermocatalytic oxidation of typical VOCs. *Appl. Catal., B* **2020**, *269*, No. 118755.

(11) Barrefors, G.; Petersson, G. Assessment of ambient volatile hydrocarbons from tobacco smoke and from vehicle emissions. *J. Chromatogr. A* **1993**, *643*, 71−76.

(12) Murphy, C. F.; Allen, D. T. Hydrocarbon emissions from industrial release events in the Houston-Galveston area and their impact on ozone formation. *Atmos. Environ.* **2005**, *39*, 3785−3798.

(13) Cano-Casanova, L.; Amorós-Pérez, A.; Ouzzine, M.; Lillo-Ródenas, M. A.; Román-Martínez, M. C. One step hydrothermal synthesis of TiO_2 with variable HCl concentration: Detailed characterization and photocatalytic activity in propene oxidation. *Appl. Catal., B* **2018**, *220*, 645−653.

(14) Amorós-Pérez, A.; Cano-Casanova, L.; Castillo-Deltell, A.; Lillo-Ródenas, M. Á.; Román-Martínez, M. C. TiO_2 modification with transition metallic species (Cr, Co, Ni, and Cu) for photocatalytic abatement of acetic acid in liquid phase and propene in gas phase. *Materials* **2018**, *12*, No. 40.

(15) Nakata, K.; Fujishima, A. TiO_2 photocatalysis: Design and applications. *J. Photochem. Photobiol., C* **2012**, *13*, 169−189.

(16) Schneider, J.; Matsuoka, M.; Takeuchi, M.; Zhang, J.; Horiuchi, Y.; Anpo, M.; Bahnemann, D. W. Understanding TiO_2 photocatalysis: Mechanisms and materials. *Chem. Rev.* **2014**, *114*, 9919−9986.

(17) Liu, G.; Yu, J. C.; Lu, G. Q.; Cheng, H. M. Crystal facet engineering of semiconductor photocatalysts: motivations, advances and unique properties. *Chem. Commun.* **2011**, *47*, No. 6763.

(18) Chen, X.; Mao, S. S. Titanium dioxide nanomaterials: Synthesis, properties, modifications, and applications. *Chem. Rev.* **2007**, *107*, 2891−2959.

(19) Ali, I.; Suhail, M.; Alothman, Z. A.; Alwarthan, A. Recent advances in syntheses, properties and applications of TiO_2 nanostructures. *RSC Adv.* **2018**, *8*, 30125−30147.

(20) Lan, Y.; Lu, Y.; Ren, Z. Mini review on photocatalysis of titanium dioxide nanoparticles and their solar applications. *Nano Energy* **2013**, *2*, 1031−1045.

(21) Zhang, W.; Li, G.; Liu, H.; Chen, J.; Ma, S.; Wen, M.; Kong, J.; An, T. Photocatalytic degradation mechanism of gaseous styrene over Au/TiO_2@ CNTs: Relevance of superficial state with deactivation mechanism. *Appl. Catal., B* **2020**, *272*, No. 118969.
(22) Leary, R.; Westwood, A. Carbonaceous nanomaterials for the enhancement of TiO_2 photocatalysis. *Carbon* **2011**, *49*, 741−772.
(23) Chen, X.; Wang, X.; Fua, X. Hierarchical macro/mesoporous TiO_2/SiO_2 and TiO_2/ZrO_2 nanocomposites for environmental photocatalysis. *Energy Environ. Sci.* **2009**, *2*, 872−877.
(24) Fernández-Catalá, J.; Cazorla-Amorós, D.; Berenguer-Murcia, Á. Facile encapsulation of P25 (TiO_2) in spherical silica with hierarchical porosity with enhanced photocatalytic properties for gas-phase propene oxidation. *Appl. Catal., A* **2018**, *564*, 123−132.
(25) Kuwahara, Y.; Sumida, Y.; Fujiwara, K.; Yamashita, H. Facile synthesis of Yolk-Shell nanostructured photocatalyst with improved adsorption properties and molecular-sieving properties. *ChemCatChem* **2016**, *8*, 2781−2788.
(26) Kuwahara, Y.; Yamashita, H. Efficient photocatalytic degradation of organics diluted in water and air using TiO_2 designed with zeolites and mesoporous silica materials. *J. Mater. Chem.* **2011**, *21*, 2407−2416.
(27) Jansson, I.; Suárez, S.; Garcia-Garcia, F. J.; Sánchez, B. Zeolite-TiO_2 hybrid composites for pollutant degradation in gas phase. *Appl. Catal., B* **2015**, *178*, 100−107.
(28) Zeng, T.; Shi, D.; Cheng, Q.; Liao, G.; Zhou, H.; Pan, Z. Construction of novel phosphonate-based MOF/P−TiO_2 heterojunction photocatalysts: enhanced photocatalytic performance and mechanistic insight. *Environ. Sci.: Nano* **2020**, *7*, 861−879.
(29) Crake, A.; Christoforidis, K. C.; Gregg, A.; Moss, B.; Kafizas, A.; Petit, C. The effect of materials architecture in TiO_2/MOF composites on CO_2 photoreduction and charge transfer. *Small* **2019**, *15*, No. 1805473.
(30) Wen, M.; Li, G.; Liu, H.; Chen, J.; An, T.; Yamashita, H. Metal−organic framework-based nanomaterials for adsorption and photocatalytic degradation of gaseous pollutants: recent progress and challenges. *Environ. Sci.: Nano* **2019**, *6*, 1006−1025.
(31) Takeda, N.; Torimoto, T.; Sampath, S.; Kuwabata, S.; Yoneyama, H. Effect of inert supports for titanium dioxide loading on enhancement of photodecomposition rate of gaseous propionaldehyde. *J. Phys. Chem. A.* **1995**, *99*, 9986−9991.
(32) Torimoto, T.; Ito, S.; Kuwabata, S.; Yoneyama, H. Effects of adsorbents used as supports for titanium dioxide loading on photocatalytic degradation of propyzamide. *Environ. Sci. Technol.* **1996**, *30*, 1275−1281.
(33) Paz, Y. Composite titanium dioxide photocatalysts and the "Adsorb & Shuttle" approach: A review. *Solid State Phenom.* **2010**, *162*, 135−162.
(34) Aprile, C.; Corma, A.; Garcia, H. Enhancement of the photocatalytic activity of TiO_2 through spatial structuring and particle size control: From subnanometric to submillimetric length scale. *Phys. Chem. Chem. Phys.* **2008**, *10*, 769−783.
(35) Liu, X.; Iu, K.; Thomas, J. K. Encapsulation of TiO_2 in zeolite Y. *J. Chem. Phys. Lett.* **1992**, *195*, 163−168.
(36) Liu, X.; Thomas, J. K. Preparation, characterization and photoreactivity of titanium (iv) oxide encapsulated in zeolites. *J. Chem. Soc., Faraday Trans.* **1993**, *89*, 1861−1865.
(37) Sampath, S.; Uchida, H.; Yoneyama, H. Photocatalytic degradation of gaseous pyridine over zeolite-supported titanium dioxide. *J. Catal.* **1994**, *149*, 189−194.
(38) Takeuchi, M.; Kimura, T.; Hidaka, M.; Rakhmawaty, D.; Anpo, M. Photocatalytic oxidation of acetaldehyde with oxygen on TiO_2/ZSM5 photocatalysts: Effect of hydrophobicity of zeolites. *J. Catal.* **2007**, *246*, 235−240.
(39) Takeuchi, M.; Hidaka, M.; Anpo, M. Efficient removal of toluene and benzene in gas phase by the TiO_2/Y-zeolite hybrid photocatalyst. *J. Hazard. Mater.* **2012**, *237*, 133−139.
(40) Kamegawa, T.; Kido, R.; Yamahana, D.; Yamashita, H. Design of TiO_2-zeolite composites with enhanced photocatalytic performances under irradiation of UV and visible light. *Microporous Mesoporous Mater.* **2013**, *165*, 142−147.
(41) Jansson, I.; Suárez, S.; García-García, F. J.; Sánchez, B. ZSM5/TiO_2 Hybrid photocatalysts: Influence of the preparation method and synergistic effect. *Top. Catal.* **2017**, *60*, 1171−1182.
(42) Huang, H.; Liu, G.; Zhan, Y.; Xu, Y.; Lu, H.; Huang, H.; Feng, Q.; Wu, M. Photocatalytic oxidation of gaseous benzene under VUV irradiation over TiO_2/Zeolites catalysts. *Catal. Today.* **2017**, *281*, 649−655.
(43) Mintova, S.; Gilson, J. P.; Valtchev, V. Advances in nanosized zeolites. *Nanoscale* **2013**, *5*, 6693−6703.
(44) Tago, T.; Konno, H.; Nakasaka, Y.; Masuda, T. Size-Controlled synthesis of nano-zeolites and their application to light olefin synthesis. *Catal. Surv. Asia* **2012**, *16*, 148−163.
(45) Puértolas, B.; Navlani-García, M.; López, J. M.; García, T.; Murillo, R.; Mastral, A. M.; Navarro, M. V.; Lozano-Castelló, D.; Bueno-López, A.; Cazorla-Amorós, D. Molecular simulation design of a multisite solid for the abatement of cold start emissions. *Chem. Commun.* **2012**, *48*, 6571−6573.
(46) Navlani-García, M.; Puértolas, B.; Lozano-Castelló, D.; Cazorla-Amorós, D.; Navarro, M. V.; García, T. CuH-ZSM-5 as hydrocarbon trap under cold start conditions. *Environ. Sci. Technol.* **2013**, *47*, 5851−5857.
(47) Puértolas, B.; Navlani-García, M.; García, T.; Navarro, M. V.; Lozano-Castelló, D.; Cazorla-Amorós, D. Optimizing the performance of catalytic traps for hydrocarbon abatement during the cold-start of a gasoline engine. *J. Hazard. Mater.* **2014**, *279*, 527−536.
(48) Nejad-Darzi, H.; Samadi-Maybodi, A.; Ghobakhluo, M. Synthesis and characterization of modified ZSM5 nanozeolite and their applications in adsorption of Acridine Orange dye from aqueous solution. *J. Porous Mater.* **2013**, *20*, 909−916.
(49) Fernández-Catalá, J.; Cano-Casanova, L.; Lillo-Ródenas, M. A.; Berenguer-Murcia, Á.; Cazorla-Amorós, D. Synthesis of TiO_2 with hierarchical porosity for the photooxidation of propene. *Molecules* **2017**, *22*, No. 2243.
(50) Fukugaichi, S.; Henmi, T.; Matsue, N. Facile synthesis of TiO_2-zeolite composite and its enhanced photocatalytic activity. *Catal. Lett.* **2013**, *143*, 1255−1259.
(51) Diebold, U.; Madey, T. E. TiO_2 by XPS. *Surf. Sci. Spectra* **1996**, *4*, 227.
(52) Etacheri, V.; Seery, M. K.; Hinder, S. J.; Pillai, S. C. Oxygen rich titania: A dopant free, high temperature stable, and visible-light active anatase photocatalyst. *Adv. Funct. Mater.* **2011**, *21*, 3744−3752.
(53) Domoroshchina, E. N.; Chernyshev, V. V.; Kuz'micheva, G. M.; Dorokhov, A. V.; Pirutko, L. V.; Kravchenko, G. V.; Chumakov, R. B. Changing the characteristics and properties of zeolite Y and nano-anatase in the formation of a nano-anatase/Y composite with improved photocatalytic and adsorption properties. *Appl. Nanosci.* **2018**, *8*, 19−31.
(54) Rico-Santacruz, M.; Serrano, E.; Marcì, G.; García-López, E. I.; García-Martínez, J. Titania-Silica materials for enhanced photocatalysis. *Chem. - Eur. J.* **2015**, *21*, 18338−18344.
(55) Ingo, G. M.; Diré, S.; Babonneau, F. XPS studies of SiO_2-TiO_2 powders prepared by sol-gel process. *Appl. Surf. Sci.* **1993**, *710*, 230−234.
(56) Suárez, S.; Jansson, I.; Ohtani, B.; Sánchez, B. From titania nanoparticles to decahedral anatase particles: Photocatalytic activity of TiO_2/zeolite hybrids for VOCs oxidation. *Catal. Today* **2019**, *326*, 2−7.
(57) Oregan, B.; Gratzel, M. A low cost, high-efficiency solar cell based on dye sensitized colloidal TiO_2 films. *Nature* **1991**, *353*, 737−740.
(58) Lillo-Ródenas, M. A.; Bouazza, N.; Berenguer-Murcia, A.; Linares-Salinas, J. J.; Soto, P.; Linares-Solano, A. Photocatalytic oxidation of propene at low concentration. *Appl. Catal., B* **2007**, *71*, 298−309.

https://dx.doi.org/10.1021/acsomega.0c04793
ACS Omega 2020, 5, 31323−31331